

## High spin states and shell model description of the neutron deficient nuclei $^{90}\text{Ru}$ and $^{91}\text{Ru}$

J. Heese, H. Grawe, K. H. Maier, and R. Schubart

*Hahn-Meitner-Institut GmbH, Glienicker Strasse 100, D-14109 Berlin, Germany*

F. Cristancho,\* C.J. Gross,† A. Jungclaus, K. P. Lieb, and D. Rudolph

*II. Physikalisches Institut, Universität Göttingen, D-37073 Göttingen, Germany*

J. Eberth and S. Skoda‡

*Institut für Kernphysik der Universität zu Köln, D-50937 Köln, Germany*

(Received 4 October 1993)

High spin states in the neutron deficient isotopes  $^{90}\text{Ru}$  and  $^{91}\text{Ru}$  have been studied in the  $2p2n$  and  $2pn$  exit channels of the reaction  $^{36}\text{Ar} + ^{58}\text{Ni}$  using the 149 MeV  $^{36}\text{Ar}$  beam at VICKSI and the OSIRIS array. By gating the  $\gamma\gamma$  coincidences with evaporated neutrons and protons, excited states in  $^{90}\text{Ru}$  were identified for the first time and the level scheme of  $^{91}\text{Ru}$  was extended. In both nuclei, the level energies and branching ratios follow the predictions of shell model calculations performed within the  $(1g_{9/2}, 2p_{1/2})$  single-particle space.

PACS number(s): 21.60.Cs, 23.20.En, 23.20.Lv, 27.60.+j

### I. INTRODUCTION

Neutron deficient nuclei with  $A=80-90$  of the  $Z=40-44$  elements encompass the borderline of the transition region between deformed nuclei (centered around  $^{76}\text{Sr}$ ) and spherical nuclei (when approaching the  $N=50$  shell closure). In this transition region, rapid nuclear shape changes with particle number or angular momentum may occur. Recent studies of neutron deficient Nb, Mo, and Tc nuclei have identified excited states in these nuclei or extended already existing level schemes [1-13]. In contrast to isotopes with  $N \leq 45$  which show features of transitional nuclei between deformed and spherical shapes (such as triaxiality and shape coexistence), the neutron deficient Mo and Tc isotopes with  $N=46-48$  are only weakly deformed and can be well described in the framework of the spherical shell model. In this paper we describe in-beam  $\gamma$ -ray studies of the isotopes  $^{90}\text{Ru}$  ( $Z = 44$ ,  $N = 46$ ) and  $^{91}\text{Ru}$  ( $Z = 44$ ,  $N = 47$ ). The ground state of  $^{91}\text{Ru}$  has been assigned  $9/2^+$  in a  $\beta^+$  and electron capture decay study [14] and an isomeric excited  $1/2^-$  state has been identified by Hagberg *et al.* [15]. However, the excitation energy of this isomer has not been determined. The occurrence of a  $9/2^+$  ground state and an excited  $1/2^-$  isomer agrees with systematics in this mass region [16]. Very recently, Arnell *et al.* reported excited states in  $^{91}\text{Ru}$  [17]. However, no detailed

model interpretations were performed in that study. We have identified excited states in  $^{90}\text{Ru}$  for the first time and extended the  $^{91}\text{Ru}$  level scheme. In addition, shell model calculations of both nuclei have been performed within a very restricted model space.

### II. EXPERIMENT AND DATA ANALYSIS

$^{90}\text{Ru}$  and  $^{91}\text{Ru}$  were produced in the reactions  $^{58}\text{Ni}(^{36}\text{Ar}, 2p2n)$  and  $^{58}\text{Ni}(^{36}\text{Ar}, 2pn)$  with a 20 mg/cm<sup>2</sup>  $^{58}\text{Ni}$  target enriched to 99.98%. The 149 MeV  $^{36}\text{Ar}$  beam was provided by the VICKSI cyclotron at the Hahn-Meitner-Institute in Berlin.  $\gamma$  rays following the heavy-ion fusion-evaporation reaction were measured with the OSIRIS spectrometer [18] consisting of 12 escape suppressed Ge detectors mounted at  $65^\circ$  and  $115^\circ$  to the beam axis. An additional large-volume Ge detector was mounted at  $162^\circ$  in order to search for Doppler broadened line shapes and  $\gamma$ -ray anisotropy ratios. Evaporated neutrons and charged particles were detected in seven NE 213 neutron detectors [19] and four 300  $\mu\text{m}$  thick  $\Delta E$  silicon surface barrier detectors, respectively. Details of the experiment have been described earlier [7,8].

In the data analysis the ratios  $R_n = I(2n\gamma)/I(n\gamma)$  and  $R_p = I(pn\gamma)/I(n\gamma)$  of  $\gamma$ -ray intensities in spectra gated with one proton and one or two neutrons have been determined and are shown in Table I for several exit channels of the reaction. It can be seen from Table I that these ratios measure the multiplicity of evaporated neutrons and protons and thus determine the exit channel of unassigned  $\gamma$  rays.

The  $\gamma\gamma$  coincidences gated with neutrons and observed in a time window of 20 ns around the prompt time peak were sorted in a  $4k \times 4k$   $E_{\gamma 1}$  vs  $E_{\gamma 2}$  matrix. The

\*Present address: Department of Physics, University of Pittsburgh, Pittsburgh, PA 15260.

†Present address: Physics Division, Oak Ridge National Laboratory, Oak Ridge, TN 37831-6371.

‡Present address: Forschungszentrum Rossendorf, Postfach 510119, D-01314 Dresden, Germany.

TABLE I. Measured ratios of  $\gamma$ -ray transitions,  $R_p = I(np\gamma)/I(n\gamma)$  and  $R_n = I(2n\gamma)/I(n\gamma)$  of nuclei in  $n$ - and  $p$ -gated spectra.

Nucleus	Exit channel	$R_p$ (%)	$R_n$ (%)
$^{90}\text{Mo}$	$4p$	27(1)	
$^{91}\text{Tc}$	$3p$	21(1)	
$^{90}\text{Tc}$	$3pn$	22(1)	5.1(2)
$^{87}\text{Mo}$	$\alpha 2pn$	18(1)	5.4(3)
$^{91}\text{Ru}$	$2pn$	17(1)	5.3(2)
$^{90}\text{Ru}$	$2p2n$	14(3)	8(2)

level schemes have been constructed from the observed coincidences and  $\gamma$ -ray intensities using the computer codes LEONE [20] and TRIXI [21]. The  $\gamma$ -ray intensities were determined from the total projection of the  $n$ - $\gamma$ -coincidence matrix. For weak transitions the intensities had to be determined from coincidence spectra and were normalized to reference transitions. No Doppler broadened line shapes were observed in the additional detector at  $162^\circ$ . Due to the weak population of the  $2p2n$  exit channel, directional correlations of oriented states (DCO) could not be determined for transitions in  $^{90}\text{Ru}$ . Therefore, the assigned spin-parities are based on systematics in this mass region and the shell model calculations. In the case of  $^{91}\text{Ru}$  the measured  $\gamma$ -anisotropy ratios of Ref. [17] and some DCO ratios from the present experiment were used in addition to these arguments. The DCO ratios

$$R_{\text{DCO}} := \frac{I(\gamma_1 \text{ at } 162^\circ; \text{ gated with } \gamma_2 \text{ at } 65^\circ, 115^\circ)}{I(\gamma_1 \text{ at } 65^\circ, 115^\circ; \text{ gated with } \gamma_2 \text{ at } 162^\circ)} \quad (1)$$

were determined from the coincidence intensities  $I(\gamma_1, \gamma_2)$ . These DCO ratios have been used to assign spins and parities to the levels as described in earlier papers [7,8,10].

### III. THE LEVEL SCHEMES OF $^{90}\text{Ru}$ AND $^{91}\text{Ru}$

#### A. $^{90}\text{Ru}$

Due to the weakness of the observed transitions, only a cascade of nine transitions in  $^{90}\text{Ru}$  could be identified. These transitions are shown in Fig. 1(a) which is a sum of  $\gamma$ - $\gamma$  coincidence spectra gated on the transitions 738, 512, 886, 773, and 291 keV. The level scheme deduced from the observed coincidences is shown in Fig. 2. The transitions have been placed in the level scheme according to their relative intensities. Due to the comparable intensities of the transitions 291, 367, 773, and 976 keV, there might be alternative orderings of these transitions and thus of the highest observed states. No evidence for noncascade or crossover transitions to other weakly populated cascades have been found. Table II summarizes the measured  $\gamma$  energies and intensities in  $^{90}\text{Ru}$ .

The energies of the most intense transitions in  $^{90}\text{Ru}$  (738, 900, 946, and 512 keV) follow very closely those in the isotope  $^{88}\text{Mo}$  (741, 914, 972, and 586 keV) [7]. Assuming the transitions of the observed cascade are decays of the yrast states, we tentatively assigned  $\pi = +$  to all observed states in  $^{90}\text{Ru}$ . In  $^{88}\text{Mo}$  [7], the sequence of  $\pi = +$  states drawing the largest  $\gamma$  flux at higher spins is the sequence  $16^+ \rightarrow 15^+ \rightarrow 14^+ \rightarrow 12^+$ . Due to the similar level schemes of both nuclei at low spins, it would be reasonable from systematics to keep the same assignments in  $^{90}\text{Ru}$ . On the other hand, the  $\gamma$ -ray branching ratios calculated in Sec. IV B rather predict a sequence  $16^+ \rightarrow 15^+ \rightarrow 13^+ \rightarrow 12^+$  of the highest observed states. The good agreement of the calculated and measured level energies in the neighboring nuclei  $^{88,89}\text{Mo}$  [7,12] and  $^{90,91}\text{Tc}$  [10,13] has shown the high predictive power of shell model calculations in this mass region. Due to the lack of experimental information in  $^{90}\text{Ru}$ , the

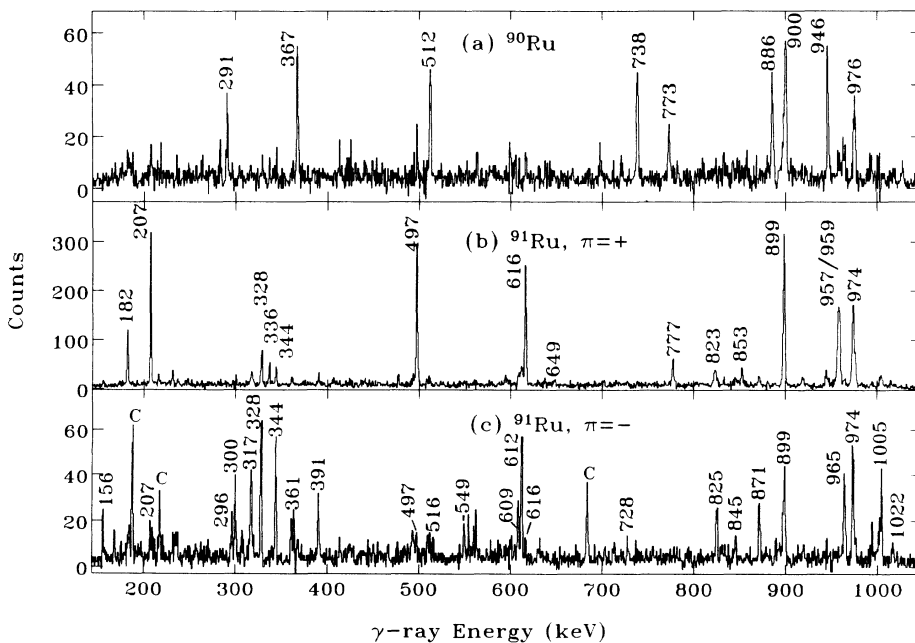


FIG. 1. Summed prompt  $n$ - $\gamma$  coincidence spectra with gates set on transitions in (a)  $^{90}\text{Ru}$ , (b)  $^{91}\text{Ru}$   $\pi = +$ , and (c)  $^{91}\text{Ru}$ ,  $\pi = -$ .  $\gamma$ -ray energies are labeled above the peaks. The spectra are not efficiency corrected. For details see text.

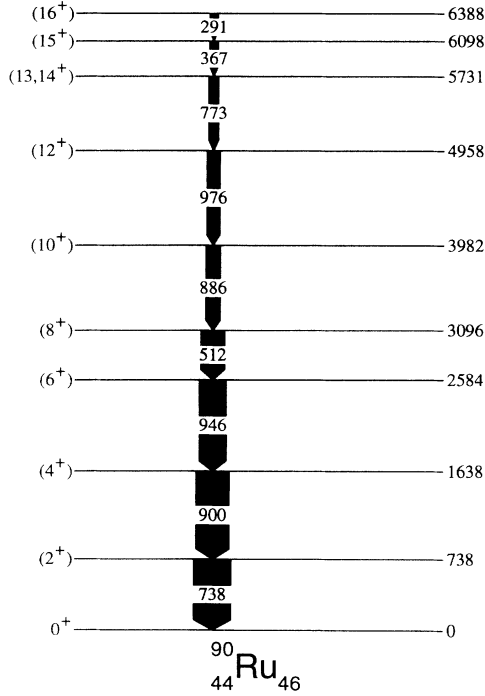


FIG. 2. Level scheme of  $^{90}\text{Ru}$  from present work. The width of the arrows measure the relative intensities of the transitions.

similarities to  $^{88}\text{Mo}$  and the results of the shell model calculations guided us in tentatively assigning spins and parities. Therefore, we tentatively assigned the spins and parities  $12^+$ ,  $(13^+, 14^+)$ ,  $15^+$ , and  $16^+$  to the highest observed states.

### B. $^{91}\text{Ru}$

A first tentative level scheme of  $^{91}\text{Ru}$  has been reported by Arnell *et al.* [17]. These authors studied  $^{91}\text{Ru}$  in the reaction  $^{58}\text{Ni}(^{40}\text{Ca}, \alpha 2pn)$  at 187 MeV.  $\gamma$  rays from excited states in  $^{91}\text{Ru}$  were assigned from  $n$ - $\gamma$  and  $\alpha$ - $\gamma$  coincidences. Spin-parity assignments of the excited states were deduced from  $\gamma$ -ray flux arguments and  $\gamma$ -ray anisotropy ratios measured in projected spectra at  $143^\circ$  and  $79(101)^\circ$  to the beam.

$^{91}\text{Ru}$  data from our experiment are shown in Figs. 1(b) and 1(c). Displayed are coincidence spectra showing transitions between the assigned positive parity states (b) and negative parity states (c). The spectrum in Fig. 1(b) is a sum of gates on the transitions 974, 497, 207, and 616 keV, while Fig. 1(c) is a spectrum coincident with the transitions 317, 609, 1005, and 1203 keV. Peaks labeled “C” in spectrum (c) denote contaminating  $^{90}\text{Tc}$   $\gamma$  rays in coincidence with the 609 keV transition [10]. The  $^{91}\text{Ru}$  level scheme deduced from these data is shown in Fig. 3. Similar to Ref. [17], all spin-parity assignments are based on indirect evidence or systematics or DCO ratios with fairly large uncertainties and are thus to be considered as tentative. Following the arguments presented in [17], we have classified the cascade of  $\gamma$  rays showing the largest  $\gamma$  flux as the positive parity sequence, the other cascade

as the negative parity sequence. Most coincidences observed in [17] have been confirmed in our study. The 1481 keV transition placed above the 7513 keV state in the previous work was very weak in our data and could not unambiguously be placed in the level scheme. In our data the line at 1203 keV in the  $\pi = -$  sequence is clearly coincident with 317 keV and all transitions depopulating

TABLE II. Level energies,  $\gamma$ -ray energies, and intensities in  $^{90}\text{Ru}$  and  $^{91}\text{Ru}$ . The  $\gamma$ -ray intensities have been measured at  $65^\circ$  and  $115^\circ$  to the beam. The errors of the  $\gamma$ -ray energies are 0.1–1.0 keV depending on the  $\gamma$ -ray energy and intensity.

$E_x$ (keV)	$E_\gamma$ (keV)	$I_\gamma$	$R_{\text{DCO}}$	Gate <sup>a</sup>	$I_i^\pi$	$\rightarrow$	$I_f^\pi$
$^{90}\text{Ru}$							
738	738.1	100(12)			$(2^+)$	$\rightarrow$	$0^+$
1638	900.1	90(14)			$(4^+)$	$\rightarrow$	$(2^+)$
2584	946.2	73(11)			$(6^+)$	$\rightarrow$	$(4^+)$
3096	511.9	64(8)			$(8^+)$	$\rightarrow$	$(6^+)$
3982	885.6	39(7)			$(10^+)$	$\rightarrow$	$(8^+)$
4958	975.6	35(5)			$(12^+)$	$\rightarrow$	$(10^+)$
5731	773.0	26(4)			$(13^+, 14^+)$	$\rightarrow$	$(12^+)$
6098	367.0	24(3)			$(15^+)$	$\rightarrow$	$(13^+, 14^+)$
6388	290.5	22(3)			$(16^+)$	$\rightarrow$	$(15^+)$
$^{91}\text{Ru}, \pi = +$							
974	973.5	100(2)	1.18(10)	B	$(13/2^+)$	$\rightarrow$	$(9/2^+)$
1872	898.6	90(5)	1.12(9)	C	$(17/2^+)$	$\rightarrow$	$(13/2^+)$
2369	497.4	41(3)	0.98(10)	B	$(21/2^+)$	$\rightarrow$	$(17/2^+)$
2985	616.1	29(3)	0.48(6)	ABC	$(23/2^+)$	$\rightarrow$	$(21/2^+)$
3192	207.2	20(1)	0.30(5)	ABC	$(25/2^+)$	$\rightarrow$	$(23/2^+)$
	822.9	15(2)	1.20(24)	C		$\rightarrow$	$(21/2^+)$
3633	648.5	3(1)			$(25/2_2^+)$	$\rightarrow$	$(23/2^+)$
	1264	4(1)				$\rightarrow$	$(21/2^+)$
3969	336.4	6(1)			$(27/2^+)$	$\rightarrow$	$(25/2_2^+)$
	777.3	10(2)	0.51(20)	C		$\rightarrow$	$(25/2^+)$
4151	959.0	35(4)	0.87(15)	ABC	$(29/2^+)$	$\rightarrow$	$(25/2^+)$
	181.8	7(2)	0.20(8)	ABC		$\rightarrow$	$(27/2^+)$
5107	957.2	23(2)	1.01(20)	ABC	$(33/2^+)$	$\rightarrow$	$(29/2^+)$
5960	852.9	10(2)			$(35/2^+)$	$\rightarrow$	$(33/2^+)$
6083	976.2	9(2)			$(37/2^+)$	$\rightarrow$	$(33/2^+)$
	123.3	4(2)				$\rightarrow$	$(35/2^+)$
7513	1430	10(3)			$(41/2^+)$	$\rightarrow$	$(37/2^+)$
$^{91}\text{Ru}, \pi = -$							
1893	919.4	13(2)			$(13/2^-)$	$\rightarrow$	$(13/2^+)$
2200	328.1	29(2)	0.81(11)	AB	$(17/2^-)$	$\rightarrow$	$(17/2^+)$
	306.9	10(2)				$\rightarrow$	$(13/2^-)$
2254	360.9	7(1)			$(15/2^-)$	$\rightarrow$	$(13/2^-)$
2409	155.6	3(2)			$(17/2_2^-)$	$\rightarrow$	$(15/2^-)$
	209.5	4(1)				$\rightarrow$	$(17/2^-)$
	516.2	4(1)				$\rightarrow$	$(13/2^-)$
2709	300.1	7(1)			$(19/2^-)$	$\rightarrow$	$(17/2_2^-)$
	509.4	4(2)				$\rightarrow$	$(17/2^-)$
2927	218	2(1)			$(19/2_2^-)$	$\rightarrow$	$(19/2^-)$
	728.0	6(1)	0.46(22)	AB	$(19/2_2^-)$	$\rightarrow$	$(17/2^-)$
3005	296.3	3(1)			$(19/2_3^-)$	$\rightarrow$	$(19/2^-)$
	804	2(1)				$\rightarrow$	$(17/2^-)$
3165	964.5	19(2)	1.15(26)	A	$(21/2^-)$	$\rightarrow$	$(17/2^-)$
	236.8	4(1)				$\rightarrow$	$(19/2_2^-)$
	455	2(1)				$\rightarrow$	$(19/2^-)$
3555	390.6	12(1)	0.54(21)	AB	$(23/2^-)$	$\rightarrow$	$(21/2^-)$
	845.4	8(1)				$\rightarrow$	$(19/2^-)$
	549.2	3(1)				$\rightarrow$	$(19/2_3^-)$
3894	339	2(1)			$(23/2_2^-)$	$\rightarrow$	$(23/2^-)$
	889.4	7(1)				$\rightarrow$	$(19/2_3^-)$
4036	871.4	18(2)	1.02(20)	AB	$(25/2^-)$	$\rightarrow$	$(21/2^-)$
	142	2(1)				$\rightarrow$	$(23/2_2^-)$
4380	343.9	15(2)	0.53(15)	AB	$(27/2^-)$	$\rightarrow$	$(25/2^-)$
	825.0	12(1)				$\rightarrow$	$(23/2^-)$
4992	612.2	23(2)	1.59(28)	AB	$(29/2^-)$	$\rightarrow$	$(27/2^-)$
	1022	2(1)				$\rightarrow$	$(27/2^+)$
5997	1004.5	20(2)			$(33/2^-)$	$\rightarrow$	$(29/2^-)$
6314	317.4	15(2)			$(35/2^-)$	$\rightarrow$	$(33/2^-)$
6922	608.5	10(1)			$(37/2^-)$	$\rightarrow$	$(35/2^-)$
7517	1203	12(2)			$(39/2^-)$	$\rightarrow$	$(35/2^-)$
8148	1226	9(2)			$(41/2^-)$	$\rightarrow$	$(37/2^-)$

<sup>a</sup>Coincidence gate A: 974 keV; B: 899 keV; C: 497 keV.

levels below the 6314 keV state, but not with the 609 and 1226 keV transitions. Therefore, this line was placed in our level scheme parallel to these transitions, leading to a new state at 7517 keV.

In Ref. [17], the energies  $E_x$  of the  $\pi = -$  states with  $2200 \text{ keV} < E_x < 3555 \text{ keV}$  could not clearly be deduced from  $\gamma\gamma$  coincidences. In the present work, a number of new transitions have been observed, giving rise to four new  $\pi = -$  states with energies  $2200 \text{ keV} < E_x < 4380 \text{ keV}$ . The observed coincidences in our study and the previously unknown connecting transitions between the  $\pi = -$  states confirmed the tentative placements by Arnell *et al.*

The presence of a connecting transition between negative and positive parity states in addition to the 328 and 919 keV  $\gamma$  rays is illustrated in Fig. 1(c) which shows a sum of gates on the transitions 317, 609, 1005, and 1203 keV. Transitions between the positive parity states can be found in this spectrum besides the 974 and 899 keV  $\gamma$  rays (e.g., 497, 616, and 207 keV). The 1022 keV transition has been identified as the decay of the  $\pi = -$  state at 4992 keV to the presumed  $I^\pi = 27/2^+$  state at 3969 keV. The energy of this transition corresponds to the sum en-

ergy of two  $e^+e^-$  annihilation  $\gamma$  rays. However, due to the small detection efficiency of a single Ge detector in OSIRIS ( $\epsilon \approx 0.05\%$  at 1 MeV  $\gamma$ -ray energy) and the short coincidence time window of 20 ns, such events are very unlikely.

Since the spin-parity assignments of the  $\pi = +$  states are well supported by intensity arguments, DCO ratios, and systematics of  $\pi = +$  states in  $^{91}\text{Ru}$  and  $^{89}\text{Mo}$  [12], an  $E1$  nature of the 1022 keV transition would give a maximum spin  $I=29/2$  of the state at 4992 keV. This is in disagreement with Arnell *et al.* who assigned  $I^\pi(4992 \text{ keV})=(31/2^-)$ . Assuming that this line is an  $E1$  transition with  $\Delta I = 1$ , we assigned  $I^\pi(4991 \text{ keV})=29/2^-$ . Arguing with the systematics of  $\pi = -$  states in  $^{91}\text{Ru}$  and  $^{89}\text{Mo}$ , the spin-parities of states with  $E_x < 4380 \text{ keV}$  in  $^{91}\text{Ru}$  have been assigned similar to Ref. [17], the spins of the  $\pi = -$  levels above 4380 keV differ by one unit from those in Ref. [17]. The multiplicities of the connecting transitions are in agreement with the previously measured  $\gamma$ -anisotropy ratios except for the 612 keV transition which was measured to have an anisotropy ratio characteristic for an  $E2$  transition in Ref. [17] but, according to our level scheme, must have  $M1$  nature.

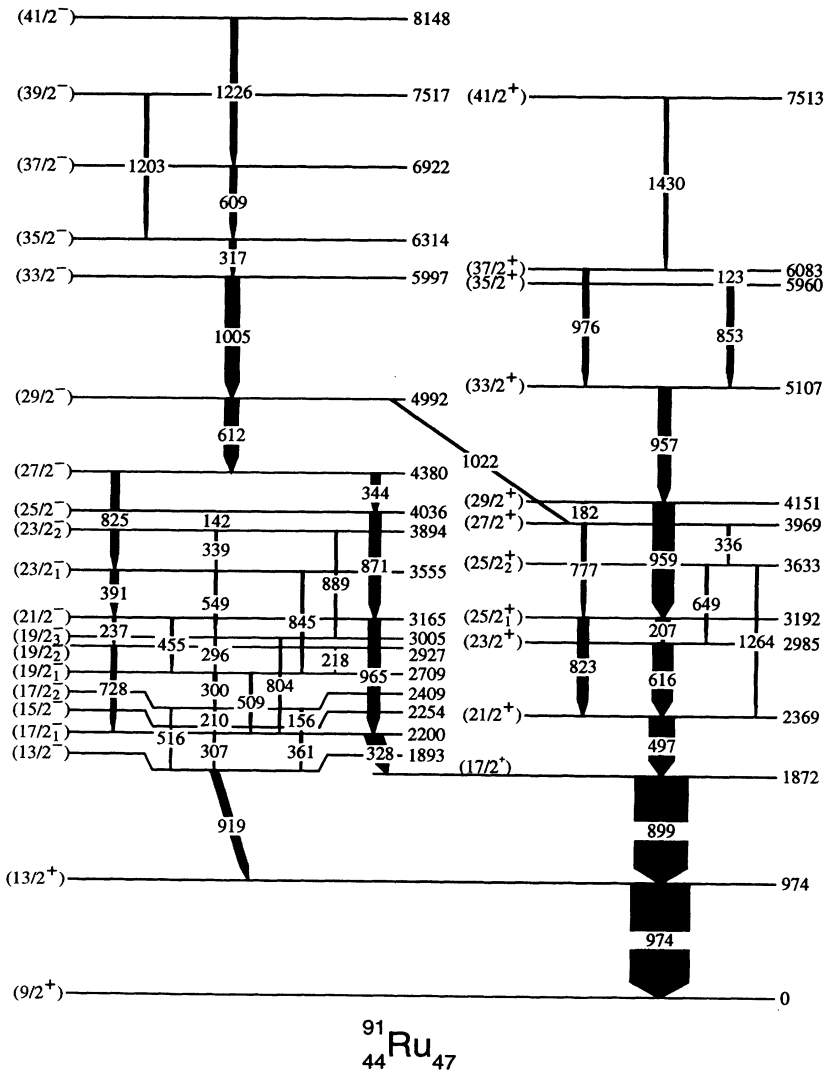


FIG. 3. Level scheme of  $^{91}\text{Ru}$ .

We note that the transitions observed in projected spectra between 609 and 612 keV show a complex structure with an additional  $E2$  component emerging from  $^{90}\text{Tc}$  [10]. The DCO ratio  $R_{\text{DCO}}=1.59(28)$  of the 612 keV  $\gamma$  ray in our data is indeed not consistent with a stretched  $E2$  transition, but indicates a  $\Delta I = 1$  transition with large  $E2$  admixture. Alternative spin-parity assignments of the  $\pi = -$  states with  $1893 \text{ keV} < E_x < 4380 \text{ keV}$  (where the DCO ratios of the connecting transitions could not be measured due to the weak intensities) would lead to greater discrepancies with the previously measured anisotropy ratios or to connecting  $M3/E4$   $\gamma$  transitions. However, more precise measurements are necessary to deduce spin-parities of the presumed  $\pi = -$  states unambiguously. The measured  $\gamma$ -ray energies, intensities and level energies in  $^{91}\text{Ru}$  are also summarized in Table II.

#### IV. DISCUSSION

##### A. Shell model level energies and wave functions

Earlier work has shown that the  $N=47$  and  $48$  nuclei of  $\text{Zr}$  ( $Z = 40$ ) and  $\text{Nb}$  ( $Z = 41$ ) can be well described by shell model calculations using a  $^{88}\text{Sr}$  core with protons and neutrons in  $g_{9/2}$  and  $p_{1/2}$  orbits [22]. In previous studies [7,10,12,13], it has been shown that this simple model space also gives good agreement in the neutron deficient  $\text{Mo}$  ( $Z=42$ ) and  $\text{Tc}$  ( $Z=43$ ) nuclei. In the present work, shell model calculations were performed with the code RITSSCHIL [23]. As in the calculations of  $^{88,89}\text{Mo}$  and  $^{90,91}\text{Tc}$  [7,12,10,13], the model space was restricted to the  $g_{9/2}$  and  $p_{1/2}$  orbits outside the semimagic  $^{88}\text{Sr}$  core. In  $^{90}\text{Ru}$  ( $^{91}\text{Ru}$ ) we have six protons above  $Z=38$  and four (three) neutron holes below the  $N=50$  shell closure. The single-particle energies and two-body matrix elements (TBME) of the residual interaction were taken from Gross and Frenkel [24] who fitted the TBME to the data of the  $N = 49$  and  $50$  isotopes of  $Z=40-44$  nuclei. In our calculations no parameter was adjusted except for shifts of the ground states which were systematically calculated to be bound too strong in all RITSSCHIL calculations for  $Z=41-43$  and  $N \leq 48$  [7,10-13]. However, the level energies relative to the calculated ground states agreed quite well with experiment. The deviations of the ground-state energies can be understood as effects of increasing deformation for  $N \leq 46$  or  $\pi(f_{5/2})$ ,  $\pi(p_{3/2})$  excitations both of which are neglected in the calculations. In order to compensate the binding energy shift, the experimental and calculated  $8^+$  energies in  $^{90}\text{Ru}$  and  $21/2^+$  energies in  $^{91}\text{Ru}$  have been aligned, leading to binding energy shifts of 497 keV in  $^{90}\text{Ru}$  and 281 keV in  $^{91}\text{Ru}$ , respectively.

Figure 4 compares the experimental and calculated level spectrum of  $^{90}\text{Ru}$ . The agreement between experiment and calculation in  $^{90}\text{Ru}$ , as measured with the mean level deviation  $\Delta E$  [24], is good ( $\Delta E=196 \text{ keV}$ ) and of the same quality as earlier results of similar calculations in the neighboring even-even nucleus  $^{88}\text{Mo}$  [7]. Positive

parity states up to spin  $I=8$  can be formed by configurations with seniority  $v=2$  and up to spin  $I=16$  with  $v=4$  ( $v = v_\pi + v_\nu$ ). However, the calculated wave functions of the yrast states show a large mixing of  $[\pi^2(v_\pi = 2), \nu^{-2}(v_\nu = 2)]$ ,  $[\pi^2(v_\pi = 2)]$  and  $[\nu^{-2}(v_\nu = 2)]$  configurations already at spin  $I=4$ . At higher spins  $I^\pi=8^+-16^+$  the configurations do not tend to correspond to two-proton or two-neutron aligned states, but mixtures of  $[\pi(g_{9/2})^2\nu(g_{9/2})^{-2}, v=4]$  configurations. This can be ascribed to the increasing strength of the proton-neutron interaction towards the middle of the  $\pi(g_{9/2})$  and  $\nu(g_{9/2})$  subshells.

In  $^{91}\text{Ru}$  the mean level deviation averaged over all states,  $\Delta E=270 \text{ keV}$ , shows that the calculation reproduces the experimental level scheme reasonably well. However, the degree of agreement between theory and experiment is very different in the  $\pi = +$  and  $\pi = -$  states as seen in Fig. 5. The calculations excellently reproduce the yrast  $\pi = +$  states ( $\Delta E=73 \text{ keV}$ ), but much less the yrast  $\pi = -$  states ( $\Delta E=410 \text{ keV}$ ). The main reason for these deviations is that the energies of the  $13/2^- - 21/2^-$  states are predicted systematically 400 - 600 keV too high. The agreement between experiment and calculation is better at higher spins.

In a recent study, Sinatkas *et al.* [25] have calculated excited states in  $N=48-50$  nuclei of  $Z=34-44$  elements using a doubly closed  $^{100}\text{Sn}$  core and a model space consisting of  $g_{9/2}$ ,  $p_{1/2}$ ,  $f_{5/2}$ , and  $p_{3/2}$  orbitals. As effective interaction, these authors used a second-order correction of the Sussex matrix elements with one-hole energies de-

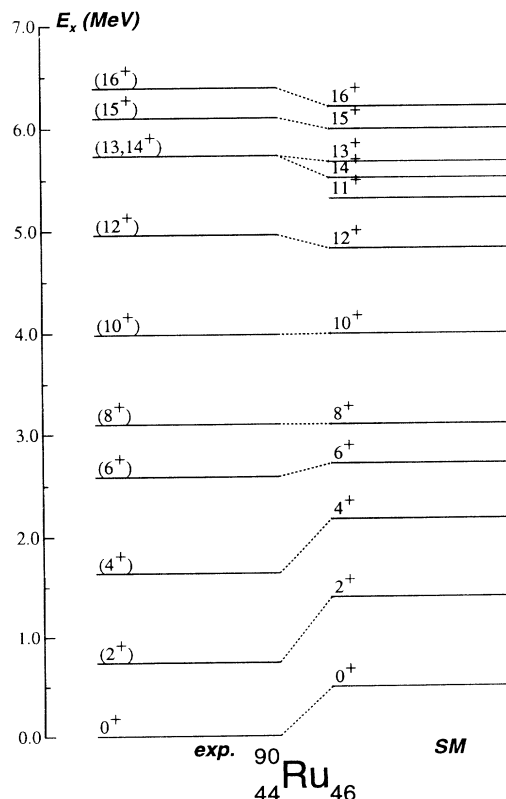


FIG. 4. Comparison of experimental and calculated level energies in  $^{90}\text{Ru}$ . The calculated states have been shifted in order to align the  $8^+$  states.

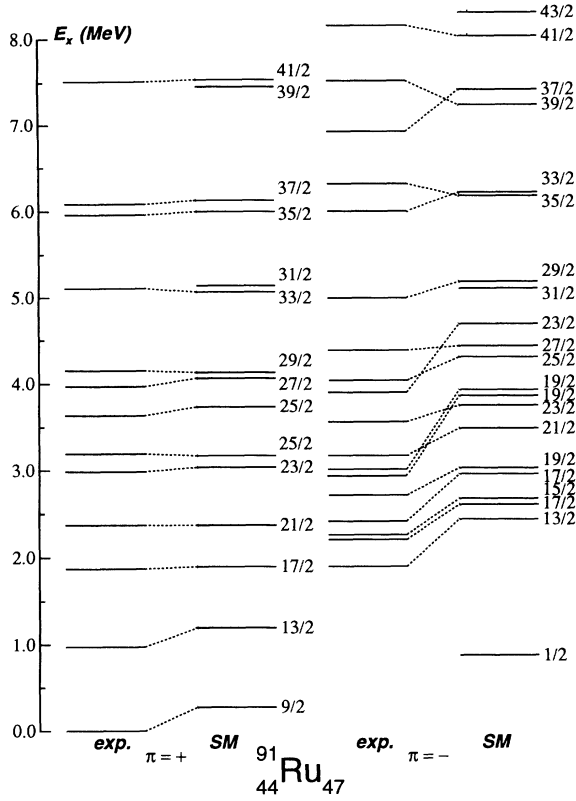


FIG. 5. Comparison of experimental and calculated level energies in  $^{91}\text{Ru}$ . The predicted energies are normalized to the  $21/2^+$  states. For details see text.

terminated from fits to over 100 levels of nuclei in this mass region. The results obtained in the odd- $A$  nuclei  $^{93}\text{Ru}$ ,  $^{93}\text{Tc}$ ,  $^{91}\text{Nb}$ ,  $^{89}\text{Zr}$ , and  $^{91}\text{Mo}$  reproduced the excitation energies of most observed states in a satisfactory manner, but the calculations also tend to predict the  $13/2^-$ – $17/2^-$  states by 300–500 keV higher than experiment. Thus the limited configuration space in our calculation might not be the reason for the observed deviations in the negative parity states.

As the  $\pi = -$  states have  $\pi(p_{1/2})\pi(g_{9/2})$  configurations (Table III), the proton  $\pi(g_{9/2})$  shell is half filled in these states, so that the clear cut coupling scheme of the  $\pi = +$  states and all other nuclei studied before in this region (i.e.,  $\pi$  particles and  $\nu$  holes) is not valid anymore. This may introduce ambiguities originating from not well-determined TBME in the interaction.

Table III lists the main components of the calculated wave functions of the  $^{91}\text{Ru}$  states. As in the calculations of  $^{89}\text{Mo}$  and  $^{91}\text{Tc}$  [12,13] the configurations contributing to the wave functions have been characterized according to their seniority. In the positive parity states, a  $\pi(g_{9/2})^2\nu(g_{9/2})^{-1}$  configuration of seniority  $v = 3$  ( $\nu_\nu=1$ ) can generate a maximum spin  $I=25/2$  and  $37/2$  with  $v=5$  ( $\nu_\nu=3$ ). The  $\pi = -$ ,  $v=3$  ( $\nu_\nu=1$ ) configuration  $\pi(p_{1/2})^1\pi(g_{9/2})^1\nu(g_{9/2})^{-1}$  reaches up to spin  $19/2$  and to  $I=31/2$  with  $v=5$  ( $\nu_\nu=3$ ). Only 3–4 partitions add up to about 60% of the total wave function. The main components of the  $^{91}\text{Ru}$  wave functions are generally very

similar to those in  $^{89}\text{Mo}$  and  $^{91}\text{Tc}$ . Exceptions are the wave functions of the  $13/2^-$ ,  $15/2^-$ ,  $17/2^-$ , and  $19/2^-$  states in  $^{91}\text{Ru}$  where strong  $v=5$  and  $v=7$  partitions are calculated.

An interesting detail of the calculations are the structures of the  $29/2^-$  and  $33/2^-$  states. In these states, a large  $v=5$  partition is realized with aligned  $\pi(g_{9/2})^2\nu(p_{1/2})^{-1}\nu(g_{9/2})^{-2}$  configurations. We note that here the negative parity is produced by a  $p_{1/2}$  neutron hole and thus the proton structure of these states is very similar to the  $\pi = +$  states.

## B. Electromagnetic transition matrix elements

Matrix elements of electromagnetic  $E2$  and  $M1$  transitions in  $^{90,91}\text{Ru}$  have been calculated with RITSSCHIL, using effective  $E2$  charges  $e_\pi=1.72$  and  $e_\nu=1.44$  and single-

TABLE III. Main partitions  $p$  and seniorities  $v$  of wave functions in  $^{91}\text{Ru}$ . The configurations are  $\nu = \nu(g_{9/2})$ ,  $\pi = \pi(g_{9/2})$ ,  $\nu' = \nu(p_{1/2})$ ,  $\pi' = \pi(p_{1/2})$ .

$I^\pi$	Configuration	$v$	$p$	(%)	$I^\pi$	Configuration	$v$	$p$	(%)
$9/2^+$	$\nu^{-1}$	1	54		$1/2^-$	$\nu'^{-1}$	1	58	
$13/2^+$	$\nu^{-3}$	3	22		$13/2^-$	$(\pi'^1\pi^3)_3$	$\nu_{7/2}^{-3}$	7	17
	$\pi_2^2$	$\nu_{9/2}^{-1}$	3	32		$(\pi'^1\pi^1)_4$	$\nu_{7/2}^{-3}$	5	16
$17/2^+$	$\pi_2^2$	$\nu_{9/2}^{-1}$	3	26		$(\pi'^1\pi^1)_4$	$\nu_{9/2}^{-1}$	3	13
	$\pi_2^2$	$\nu_{13/2}^{-3}$	5	17		$(\pi'^1\pi^1)_5$	$\nu_{7/2}^{-3}$	5	13
$21/2^+$	$\pi_8^2$	$\nu_{9/2}^{-1}$	3	22	$15/2^-$	$(\pi'^1\pi^1)_4$	$\nu_{7/2}^{-3}$	5	22
	$\pi_4^2$	$\nu_{13/2}^{-3}$	5	13		$(\pi'^1\pi^1)_5$	$\nu_{7/2}^{-3}$	5	22
	$\pi_8^2$	$\nu_{9/2}^{-1}$	3	11		$(\pi'^1\pi^3)_3$	$\nu_{9/2}^{-1}$	5	14
	$\pi_8^2$	$\nu_{13/2}^{-3}$	5	17	$17/2_1^-$	$(\pi'^1\pi^1)_5$	$\nu_{9/2}^{-1}$	3	26
$23/2^+$	$\pi_8^2$	$\nu_{9/2}^{-1}$	3	43		$(\pi'^1\pi^1)_4$	$\nu_{9/2}^{-1}$	3	18
	$\pi_8^2$	$\nu_{7/2}^{-3}$	5	9	$17/2_2^-$	$(\nu'^{-1}\nu^{-2})_{17/2}$		3	46
$25/2_1^+$	$\pi_8^2$	$\nu_{9/2}^{-1}$	3	53	$19/2^-$	$(\pi'^1\pi^1)_5$	$\nu_{9/2}^{-1}$	3	53
	$\pi_8^2$	$\nu_{13/2}^{-3}$	5	16		$(\pi'^1\pi^3)_7$	$\nu_{7/2}^{-3}$	7	10
$25/2_2^+$	$\pi_8^2$	$\nu_{9/2}^{-1}$	3	16	$21/2^-$	$(\pi'^1\pi^3)_7$	$\nu_{9/2}^{-1}$	5	24
	$\pi_4^2$	$\nu_{17/2}^{-3}$	5	12		$(\pi'^1\pi^3)_6$	$\nu_{9/2}^{-1}$	5	11
	$\pi_6^2$	$\nu_{13/2}^{-3}$	5	12	$23/2^-$	$(\pi'^1\pi^3)_7$	$\nu_{9/2}^{-1}$	5	40
	$\pi_8^2$	$\nu_{13/2}^{-3}$	5	10		$(\pi'^1\pi^1)_5$	$\nu_{13/2}^{-3}$	5	25
$27/2^+$	$\pi_8^2$	$\nu_{13/2}^{-3}$	5	24	$25/2^-$	$(\pi'^1\pi^3)_9$	$\nu_{9/2}^{-1}$	5	22
	$\pi_{10}^4$	$\nu_{9/2}^{-1}$	5	22		$(\pi'^1\pi^3)_8$	$\nu_{9/2}^{-1}$	5	10
	$\pi_8^2$	$\nu_{11/2}^{-3}$	5	18	$27/2^-$	$(\pi'^1\pi^3)_9$	$\nu_{9/2}^{-1}$	5	39
$29/2^+$	$\pi_8^2$	$\nu_{13/2}^{-3}$	5	42		$(\pi'^1\pi^3)_7$	$\nu_{13/2}^{-3}$	7	24
	$\pi_{10}^4$	$\nu_{9/2}^{-1}$	5	22		$(\pi'^1\pi^1)_5$	$\nu_{17/2}^{-3}$	5	8
	$\pi_6^2$	$\nu_{17/2}^{-3}$	5	12	$29/2^-$	$(\pi'^1\pi^3)_{11}$	$\nu_{9/2}^{-1}$	5	28
$33/2^+$	$\pi_8^2$	$\nu_{17/2}^{-3}$	5	33		$(\nu'^{-1}\nu^{-2})_{17/2}$		5	25
	$\pi_{10}^4$	$\nu_{13/2}^{-3}$	7	25	$33/2^-$	$\pi_8^2$	$(\nu'^{-1}\nu^{-2})_{17/2}$	5	76
	$\pi_6^2$	$\nu_{21/2}^{-3}$	5	12		$(\pi'^1\pi^3)_{11}$	$\nu_{13/2}^{-3}$	7	4
$35/2^+$	$\pi_8^2$	$\nu_{21/2}^{-3}$	5	59	$35/2^-$	$(\pi'^1\pi^3)_{11}$	$\nu_{13/2}^{-3}$	7	42
	$\pi_7^4$	$\nu_{21/2}^{-3}$	7	10		$(\pi'^1\pi^3)_9$	$\nu_{17/2}^{-3}$	7	24
	$\pi_{10}^4$	$\nu_{17/2}^{-3}$	7	9		$(\pi'^1\pi^3)_{13}$	$\nu_{9/2}^{-1}$	5	18
$37/2^+$	$\pi_8^2$	$\nu_{21/2}^{-3}$	5	66	$37/2^-$	$(\pi'^1\pi^3)_9$	$\nu_{21/2}^{-3}$	7	33
	$\pi_{10}^4$	$\nu_{17/2}^{-3}$	7	22		$(\pi'^1\pi^3)_8$	$\nu_{21/2}^{-3}$	7	26
$41/2^+$	$\pi_{10}^4$	$\nu_{21/2}^{-3}$	7	67		$(\pi'^1\pi^3)_{11}$	$\nu_{17/2}^{-3}$	7	26
	$\pi_{12}^4$	$\nu_{17/2}^{-3}$	7	21	$39/2^-$	$(\pi'^1\pi^3)_{11}$	$\nu_{17/2}^{-3}$	7	41
						$(\pi'^1\pi^3)_9$	$\nu_{21/2}^{-3}$	7	40
						$(\pi'^1\pi^5)_{13}$	$\nu_{13/2}^{-3}$	9	15

TABLE IV. Measured and calculated  $\gamma$ -ray branching ratios of states in  $^{90}\text{Ru}$  and  $^{91}\text{Ru}$ 

$E_x$ (keV)	$E_\gamma$ (keV)	$I_i^\pi$	$I_f^\pi$	$M_\gamma$	$b_{\text{exp}}^a$ (%)	$b_{\text{SM}}^b$ (%)
$^{90}\text{Ru}$						
6388	291	(16 <sup>+</sup> )	(15 <sup>+</sup> )	$M1/E2$	100	89
	692 <sup>c</sup>		(14 <sup>+</sup> )	$E2$	n.o. <sup>d</sup>	11
6098 <sup>e</sup>	474 <sup>e</sup>	(15 <sup>+</sup> )	(14 <sup>+</sup> )	$M1/E2$	n.o.	22
	367		(13 <sup>+</sup> )	$E2$	100	78
6098 <sup>f</sup>	367	(15 <sup>+</sup> )	(14 <sup>+</sup> )	$M1/E2$	100	21
	318 <sup>e</sup>		(13 <sup>+</sup> )	$E2$	n.o.	79
5731 <sup>e</sup>	773	(13 <sup>+</sup> )	(12 <sup>+</sup> )	$M1/E2$	100	99.7
	356 <sup>e</sup>		(11 <sup>+</sup> )	$E2$	n.o.	0.3
5731 <sup>f</sup>	773	(14 <sup>+</sup> )	(12 <sup>+</sup> )	$E2$	100	83
	156 <sup>e</sup>		(13 <sup>+</sup> )	$M1/E2$	n.o.	17
$^{91}\text{Ru}, \pi = +$						
6083	123	(37/2 <sup>+</sup> )	(35/2 <sup>+</sup> )	$M1/E2$	30(15)	17
	976		(33/2 <sup>+</sup> )	$E2$	70(15)	83
4151	182	(29/2 <sup>+</sup> )	(27/2 <sup>+</sup> )	$M1/E2$	17(5)	21
	518		(25/2 <sup>+</sup> )	$E2$	n.o.	0.04
	959		(25/2 <sup>+</sup> )	$E2$	83(5)	79
3969	336	(27/2 <sup>+</sup> )	(25/2 <sup>+</sup> )	$M1/E2$	38(8)	28
	777		(25/2 <sup>+</sup> )	$M1/E2$	62(8)	50
	984		(23/2 <sup>+</sup> )	$E2$	n.o.	22
3633	649	(25/2 <sup>+</sup> )	(23/2 <sup>+</sup> )	$M1/E2$	40(15)	41
	441		(25/2 <sup>+</sup> )	$M1/E2$	n.o.	14
	1264		(21/2 <sup>+</sup> )	$E2$	60(15)	45
3192	207	(25/2 <sup>+</sup> )	(23/2 <sup>+</sup> )	$E2/M1$	60(10)	58
	823		(21/2 <sup>+</sup> )	$E2$	40(10)	42
$^{91}\text{Ru}, \pi = -$						
8148	1226	(41/2 <sup>-</sup> )	(37/2 <sup>-</sup> )	$E2$	100	72
	632		(39/2 <sup>-</sup> )	$M1/E2$	n.o.	28
7517	1203	(39/2 <sup>-</sup> )	(35/2 <sup>-</sup> )	$E2$	100	19
	595		(37/2 <sup>-</sup> )	$M1/E2$	n.o.	81
6922	609	(37/2 <sup>-</sup> )	(35/2 <sup>-</sup> )	$M1/E2$	100	98
	925		(33/2 <sup>-</sup> )	$E2$	n.o.	2
5997	1005	(33/2 <sup>-</sup> )	(29/2 <sup>-</sup> )	$E2$	100	87
	1112 <sup>e</sup>		(31/2 <sup>-</sup> )	$M1/E2$	n.o.	13
4992	956	(29/2 <sup>-</sup> )	(25/2 <sup>-</sup> )	$E2$	n.o.	62
	612		(27/2 <sup>-</sup> )	$M1/E2$	100	38
4380	825	(27/2 <sup>-</sup> )	(23/2 <sup>-</sup> )	$E2$	44(6)	32
	344		(25/2 <sup>-</sup> )	$M1/E2$	56(6)	68
4036	871	25/2 <sup>-</sup>	21/2 <sup>-</sup>	$E2$	90(5)	62
	480		23/2 <sup>-</sup>	$M1/E2$	n.o.	30
	142		23/2 <sup>-</sup>	$M1/E2$	10(5)	8
3894	889	(23/2 <sup>-</sup> )	(19/2 <sup>-</sup> )	$E2$	76(12)	85
	729		(21/2 <sup>-</sup> )	$M1/E2$	n.o.	9
	339		(23/2 <sup>-</sup> )	$M1/E2$	24(12)	5
3555	845	(23/2 <sup>-</sup> )	(19/2 <sup>-</sup> )	$E2$	34(8)	21
	391		(21/2 <sup>-</sup> )	$E2$	52(8)	78
	628		(19/2 <sup>-</sup> )	$E2$	n.o.	0.2
	549		(19/2 <sup>-</sup> )	$M1/E2$	14(6)	0.02
3165	965	(21/2 <sup>-</sup> )	(17/2 <sup>-</sup> )	$E2$	78(7)	78
	755		(17/2 <sup>-</sup> )	$E2$	n.o.	0.7
	455		(19/2 <sup>-</sup> )	$M1/E2$	8(5)	14
	237		(19/2 <sup>-</sup> )	$M1/E2$	14(4)	7
3005	750	(19/2 <sup>-</sup> )	(15/2 <sup>-</sup> )	$E2$	n.o.	9
	804		(17/2 <sup>-</sup> )	$M1/E2$	44(16)	44
	595		(17/2 <sup>-</sup> )	$M1/E2$	n.o.	37
	296		(19/2 <sup>-</sup> )	$M1/E2$	56(16)	10
2927	673	(19/2 <sup>-</sup> )	(15/2 <sup>-</sup> )	$E2$	n.o.	10
	728		(17/2 <sup>-</sup> )	$M1/E2$	76(12)	52
	518		(17/2 <sup>-</sup> )	$M1/E2$	n.o.	38
	218		(19/2 <sup>-</sup> )	$M1/E2$	24(12)	0.1
2709	509	(19/2 <sup>-</sup> )	(17/2 <sup>-</sup> )	$M1/E2$	38(10)	99
	300		(17/2 <sup>-</sup> )	$M1/E2$	62(10)	1
2409	516	(17/2 <sup>-</sup> )	(13/2 <sup>-</sup> )	$E2$	32(11)	0.5
	156		(15/2 <sup>-</sup> )	$M1/E2$	28(14)	3.5
	210		(17/2 <sup>-</sup> )	$M1/E2$	40(9)	96

<sup>a</sup>Branching ratios determined from measured  $\gamma$ -ray intensities.

<sup>b</sup>Calculated branching ratios.

<sup>c</sup>Calculated transition energy.

<sup>d</sup>Not observed in experiment.

<sup>e</sup>Assuming  $I^\pi(5731 \text{ keV})=13^+$ .

<sup>f</sup>Assuming  $I^\pi(5731 \text{ keV})=14^+$ .

particle  $M1$  moments deduced from  $g$  factors of  $p_{1/2}$  and  $g_{9/2}$  states in  $N \approx 50$  nuclei [26] as described in Ref. [13]. From these matrix elements, branching ratios of  $\gamma$  decays have been determined using the experimental transition energies. Table IV compares the calculated branching ratios to experimental values deduced from the  $\gamma$ -ray intensities measured at 90° and 115° to the beam. As the intensities have not been corrected for angular distributions, the deduced branching ratios might have systematic errors as large as 20%. However, the strongest  $\gamma$ -decay paths should follow the shell model predictions.

In  $^{90}\text{Ru}$  the predicted  $15^+ \rightarrow 14^+$  transition matrix element is very small, the most probable transition is  $15^+ \rightarrow 13^+$ . However, the most likely spin of the 5731 keV state from systematics is  $I^\pi=14^+$ . With both assignments of the 5731 keV state, good agreement between calculated and experimental level energies is achieved.

The calculated energies and branching ratios of the  $^{91}\text{Ru}$   $\pi = +$  states are in good agreement with experiment. In the  $\pi = -$  states, most of the predicted branching ratios are also observed within the experimental uncertainties. The values disagree for the transitions  $41/2^- \rightarrow 39/2^-$ ,  $39/2^- \rightarrow 37/2^-$ ,  $29/2^- \rightarrow 25/2^-$ ,  $25/2^- \rightarrow 23/2^-$ ,  $19/2_3^- \rightarrow 17/2_2^-$ , and  $19/2_2^- \rightarrow 17/2_2^-$ , where strong decay branches are predicted but not observed. On the other hand, the transitions  $23/2^- \rightarrow 19/2_3^-$ ,  $19/2_2^- \rightarrow 19/2_1^-$ ,  $19/2^- \rightarrow 17/2^-$ , and  $17/2_2^- \rightarrow 13/2, 15/2^-$  are experimentally much stronger than predicted. Most of the discrepancies occur in the region of high level density between 1893 and 3005 keV and  $13/2^- \leq I^\pi \leq 19/2^-$ . Experimentally, here the  $\gamma$ -ray flux is spread over many decay branches with low intensity which eventually may escape observation (see Fig. 3). Theoretically, these states are characterized by a coupling of the  $\nu(g_{9/2})_{9/2,7/2}^{-3}$  configuration of seniority  $\nu_\nu=1,3$  to the  $\pi(p_{1/2}, g_{9/2})_{4,5}$  multiplet (see Table III) which, due to the half-filled  $\pi(g_{9/2})$  shell, is governed by a nearly degenerate  $\pi(g_{9/2})\nu(g_{9/2})^{-1}$  multiplet. This gives rise to close-lying highly mixed yrast and yrare states of identical spin, which are subject to fluctuations in level order and configuration caused by uncertainties of the effective residual interaction.

## V. CONCLUSIONS

In this paper, excited states in  $^{90}\text{Ru}$  have been studied for the first time and a level scheme was established up to 6.4 MeV excitation energy and probable spin  $I^\pi=16^+$ , corresponding to  $8\hbar$  below the maximum spin  $I_{\text{max}}=24\hbar$  in the  $(g_{9/2})$  model space. In  $^{91}\text{Ru}$ , the negative parity states were observed up to an excitation energy of 8.2 MeV, the positive parity states up to 7.2 MeV and spin  $41/2^\pm$ ,  $(2-3)\hbar$  below  $I_{\text{max}}$  in the  $(g_{9/2}, p_{1/2})$  space. The level scheme of Ref. [17] was confirmed and extended by 12 transitions and 4 new states.

Shell model calculations in the restricted  $(g_{9/2}, p_{1/2})$  model space have been carried out and gave good agree-

ment with experiment in the yrast  $\pi = +$  states of both nuclei. The results in  $\pi = -$  states of  $^{91}\text{Ru}$  are slightly worse. The  $I^\pi = 13/2^- - 21/2^-$  energies are predicted to be 300–500 keV higher compared with experiment and the predicted  $\gamma$  decays of these states disagree with experiment. However, the main properties of the  $^{91}\text{Ru}$  level

scheme are still reproduced within the  $(g_{9/2}, p_{1/2})$  model space.

#### ACKNOWLEDGMENT

This work was supported in part by Deutsches BMFT.

- 
- [1] C.J. Gross, K.P. Lieb, D. Rudolph, M.A. Bentley, W. Gelletly, H.G. Price, J. Simpson, D.J. Blumenthal, P.J. Ennis, C.J. Lister, Ch. Winter, J.L. Durell, B.J. Varley, Ö. Skeppstedt, and S. Rastikerdar, Nucl. Phys. **A535**, 203 (1991); Phys. Rev. C **44**, R2253 (1991).
- [2] A. Jungclaus, K.P. Lieb, C.J. Gross, J. Heese, D. Rudolph, D.J. Blumenthal, P. Chowdhury, P.J. Ennis, C.J. Lister, Ch. Winter, J. Eberth, S. Skoda, M.A. Bentley, W. Gelletly, and B.J. Varley, Z. Phys. A **340**, 125 (1991).
- [3] W. Gelletly, M.A. Bentley, H.G. Price, J. Simpson, C.J. Gross, B.J. Varley, Ö. Skeppstedt, and S. Rastikerdar, Phys. Lett. B **253**, 287 (1991).
- [4] Ch. Winter *et al.*, Phys. Lett. B **258**, 289 (1991); Nucl. Phys. **A535**, 137 (1991).
- [5] D. Rudolph, F. Cristancho, C.J. Gross, A. Jungclaus, K.P. Lieb, M.A. Bentley, W. Gelletly, J. Simpson, H. Grawe, J. Heese, K.H. Maier, J. Eberth, S. Skoda, J.L. Durell, B.J. Varley, D.J. Blumenthal, C.J. Lister, and S. Rastikerdar, J. Phys. G **17**, L113 (1991).
- [6] D. Rudolph, F. Cristancho, C.J. Gross, A. Jungclaus, K.P. Lieb, H. Grawe, J. Heese, K.H. Maier, J. Eberth, and S. Skoda, Z. Phys. A **342**, 121 (1992).
- [7] M. Weiszflog, K.P. Lieb, F. Cristancho, C.J. Gross, A. Jungclaus, D. Rudolph, H. Grawe, J. Heese, K.H. Maier, R. Schubart, J. Eberth, and S. Skoda, Z. Phys. A **342**, 257 (1992).
- [8] M.K. Kabadiyski, F. Cristancho, C.J. Gross, A. Jungclaus, K.P. Lieb, D. Rudolph, H. Grawe, J. Heese, K.H. Maier, J. Eberth, S. Skoda, W.T. Chou, and E.K. Warburton, Z. Phys. A **343**, 165 (1992).
- [9] P. Singh, R.G. Pillay, J.A. Sheikh, and H.G. Devare, Phys. Rev. C **45**, 2161 (1992).
- [10] D. Rudolph, C.J. Gross, M.K. Kabadiyski, K.P. Lieb, M. Weiszflog, H. Grawe, J. Heese, K.H. Maier, and J. Eberth, Phys. Rev. C **47**, 2574 (1993).
- [11] A. Bödeker, K.P. Lieb, C.J. Gross, M.K. Kabadiyski, D. Rudolph, M. Weiszflog, J. Eberth, H. Grawe, J. Heese, and K.H. Maier, Phys. Rev. C **48**, 1617 (1993).
- [12] M. Weiszflog, D. Rudolph, C.J. Gross, M.K. Kabadiyski, K.P. Lieb, H. Grawe, J. Heese, K.H. Maier, and J. Eberth, Z. Phys. A **344**, 395 (1993).
- [13] D. Rudolph, C.J. Gross, A. Harder, M.K. Kabadiyski, K.P. Lieb, M. Weiszflog, J. Altmann, A. Dewald, J. Eberth, T. Mylaeus, H. Grawe, J. Heese, and K.H. Maier, Phys. Rev. C **49**, 66 (1994).
- [14] P. Komninos, E. Nolte, and P. Blasi, Z. Phys. A **314**, 135 (1983).
- [15] E. Hagberg, J.C. Hardy, H. Schmeing, E.T.H. Clifford, and V.T. Koslowsky, Nucl. Phys. **A395**, 12 (1983).
- [16] C.M. Lederer and V.S. Shirley, *Table of Isotopes*, 7th ed. (Wiley, New York, 1978).
- [17] S.E. Arnell, D. Foltescu, H.A. Roth, Ö. Skeppstedt, A. Nilsson, S. Mitarai, and J. Nyberg, Phys. Scr. **47**, 355 (1993).
- [18] R.M. Lieder, H. Jäger, A. Neskakis, and T. Venkova, Nucl. Instrum. Methods **220**, 363 (1984).
- [19] D. Alber, H. Grawe, H. Haas, and B. Spellmeyer, Nucl. Instrum. Methods **263**, 401 (1988).
- [20] S. Albers, A. Clauberg, A. Dewald, C. Wesselborg, and A. Zilges, Verhandl. DPG (VI) **23**, 227 (1988).
- [21] H. Wolters, program TRIXI, University of Cologne, 1988 (unpublished).
- [22] K. Oxorn, S.K. Mark, J.E. Kitching, and S.S.M. Wong, Z. Phys. A **321**, 485 (1985).
- [23] D. Zwarts, Comp. Phys. Commun. **38**, 365 (1985).
- [24] R. Gross and A. Frenkel, Nucl. Phys. **A267**, 85 (1976).
- [25] J. Sinatkas, L.D. Skouras, D. Strottman, and J.D. Vergados, J. Phys. G **18**, 1377 (1992).
- [26] P. Raghavan, At. Data Nucl. Data Tables **42**, 189 (1989).